Removal of enalapril maleate drug from industry waters using activated biochar prepared from *Butia capitata* seed. Kinetics, equilibrium, thermodynamic, and DFT calculations

Mariene R. Cunha[1], Mu. Naushad[2], Miguel Ponce-Vargas[3], Eder C. Lima[1,4*], Farooq Sher[5], Navid Rabiee[6], Dison S.P. Franco[7], Pascal S. Thue[8], Hai Nguyen Tran[9,10], Michael Badawi[11]

[1-] *Mine, Metallurgical, and Materials Engineering Postgraduate program (PPGE3M). School of Engineering, Federal University of Rio Grande do Sul (UFRGS), Av. Bento Gonçalves 9500, Porto Alegre, RS, Brazil*

[2-] *Department of Chemistry, College of Science, Building #5, King Saud University, P.O. Box 2455, Riyadh 11451, Saudi Arabia*

[3-] *Institut de Chimie Moléculaire de Reims, UMR CNRS 7312, Université de Reims Champagne-Ardenne, Moulin de la Housse, Reims 51687, France*

[4-] *Institute of Chemistry, Federal University of Rio Grande do Sul (UFRGS), Av. Bento Gonçalves 9500, Porto Alegre, RS, Brazil*

[5-] *Department of Engineering, Nottingham Trent University, Nottingham NG11 8NS, United Kingdom.*

[6-] *Centre for Molecular Medicine and Innovative Therapeutics, Murdoch University, Perth, WA 6150, Australia.*

[7-] *Department of Civil and Environmental. Universidad de la Costa, CUC, Calle 58 # 55–66, Barranquilla, Atlántico, Colombia.*

[8-] *Environmental Science Graduate Program, Engineering Center, Federal University of Pelotas (UFPel), Pelotas, RS, Brazil*

[9-] *Center for Energy and Environmental Materials, Institute of Fundamental and Applied Sciences, Duy Tan University, Ho Chi Minh City, 700000, Vietnam*

[10-] *Faculty of Environmental and Chemical Engineering, Duy Tan University, Da Nang City, 550000, Vietnam*

[11-] *Laboratoire de Physique et Chimie Théoriques, CNRS, Université de Lorraine, Nancy, F-54000, France*

* corresponding author: profederlima@gmail.com; eder.lima@ufrgs.br

Abstract

Porous biochar was fabricated from *Butia capitata* (Bc) seed, which was used to uptake enalapril maleate from synthetic wastewater. Activated biochars were fabricated by blending Bc and $ZnCl_2$ at 1:1 (BcB-1.0) or 1:1.5 (BcB-1.5) proportions and furtherly pyrolyzed at 600°C. The elemental analysis, Boehm titration, hydrophobic balance ratio, FTIR, TGA, and N_2 isotherm characterized the carbon-based materials. They presented a hydrophilic behavior with diverse polar groups on their surface. BcB-1 and BcB-1.5 biochars have a total pore volume of 0.392 and 0.492 $cm^3\,g^{-1}$ and a surface area of 1267 and 1520 $m^2\,g^{-1}$, respectively. The kinetics and isothermal data were adequately adjusted to the fractal-like pseudo-second-order and Liu models. The employment of BcB-1.0 and BcB-1.5 for treating synthetic wastewater containing high levels of pollutants had elevated efficiency in their removals (up to 99.06%). We conducted a computational study, density functional theory (DFT), to examine the interactions between enalapril and a graphitic domain of biochar. By using these calculations, the most stable configuration presented interaction energy of -88.7 kJ mol^{-1} implies a face-to-face π–π stacking interaction involving the enalapril phenyl segment and an aromatic ring of biochar, as well as London dispersion arising from the proximity of ethoxy/pyrrolidine to biochar carbon atoms, with interatomic distances of 3.31 Å for the former and 3.60 Å /3.48 Å for the latter. Also, the DFT calculations agreed with the thermodynamic data calculated from the isotherms (283-318 K).

Keywords: activated biochar; synthetic effluents; *a*dsorption mechanism, emerging contaminant; density functional theory

1. Introduction

Medicines are employed mainly to ameliorate the life quality of humanity by treating diseases and extending long life. Notwithstanding, the increased employment of drug substances causes their discharge into the environment. The source of pharmaceutical contamination comes from hospital effluents [1], the pharmaceutical industry [2], and excretions of livestock animals and domestic sewage [1,3]. Also, the discharge of pharmaceuticals into the waters is an environmental apprehension [1,4] due to these chemicals can influence living organisms and threaten the water quality for human consummation [1,4].

Pharmaceuticals are categorized as emerging contaminants [4,5]. These species are any natural or synthetic pollutants found in water sources that are not systematically controlled by Environmental agencies, which may cause living beings impacts or ecological effects [4,5].

Conventional water and wastewater treatment contaminated with pharmaceuticals are usually performed using biological treatment [6,7], photocatalysis [8,9], Fenton-like processes [10,11], electrochemical degradation [12,13], membrane filtration [14,15], ultrasound degradation [16,17], and adsorption [18-23]. Exception for adsorption, these treatment methods have weaknesses, such as high implemental costs, high sludge production [24], and forming transformation products that present higher toxicity than the parent pollutant [25]. In this sense, it is crucial to develop efficient adsorption methods to uptake organic compounds from water with a low implementation cost and high efficiency [26,27].

Enalapril is often utilized to treat hypertension and heart failure. Enalapril is in a class of medications called angiotensin-converting enzyme inhibitors [28]. Enalapril decreases some substances that tighten the blood vessels [28,29]. Enalapril is also sometimes used to treat kidney disease related to diabetes [28,29]. In Brazil, this drug is available for free for treating hypertension problems through the Brazillian Pharmacy Programs [30].

As the population largely employs this pharmaceutical, it is necessary to develop methods

for its removal from water and pharmaceutical wastewater. On the other hand, few reports in the literature cite enalapril as an adsorbate [26,31]. However, there is no study for removing this drug (a solute adsorbate) from water and wastewater. Thus, due to the high use of enalapril as a pharmaceutical and the few adsorption studies of enalapril as an adsorbate, it is crucial to produce new efficient adsorbents for enalapril uptake from pharmaceutical industry wastewater.

Using carbon-based materials to remove drugs is a hot subject in the adsorption literature [1,19,20,21,27,32,33] because these carbon materials are usually prepared using residual biomass. This waste material is usually pyrolyzed in an inert atmosphere producing a carbon material called biochar [19,23,27,32,33]. Biochar can be used without activation. Alternatively, it could be activated, producing carbon material with improved textural characteristics and high sorption capacities close to expensive adsorbents such as activated carbon, graphenes, carbon nanotubes, etc. [1,19,23,27,32].

The *Butia capitata* (Bc) seeds were employed in this research to fabricate activated biochar. The *Butia Arecaceae family owns the Butia capitata* is found in the Brazillian vegetation [34]. The species' fruits are rich in vitamins and carbohydrates and are crucial for preserving native vegetation [34]. In addition, they are employed in preparing ice cream and juices [34]. However, the *Butia capitata* fruits are utilized for producing food. Therefore, the seeds are discarded, impelling new research for utilizing this residual biomass as a carbon source for fabricating biochar for wastewater treatment.

This paper aims to use *Butia capitata* (Bc) seeds (agro-industrial waste) to produce activated biochars (BcB-1.0 and BcB-1.5) for the removal of an emerging contaminant (enalapril). This pharmaceutical is often utilized to treat hypertension and heart failure, and also this drug is available for free for treating hypertension problems through the Brazillian Pharmacy Programs.

In this work, *Butia capitata* seeds (Bc) were used as a carbon precursor for biochar production. The biochars were characterized by different analytical techniques such as FTIR,

adsorption and desorption isotherms of N_2, Bohem titration, organic elemental analysis, $pH_{pzc,}$ and hydrophobic balance ratio (HI). In addition, the adsorption kinetics, equilibrium, and thermodynamics assays with enalapril in the biochars were attained, and the enalapril adsorption mechanisms onto the carbon materials were proposed. The interaction between biochar and enalapril has also been investigated at the molecular scale using density functional theory (DFT) calculations. After these studies, the activated biochars efficiently removed enalapril from aqueous effluents and simulated pharmaceutical industrial wastewater (removal up to 99.06%). This achievement is the main contribution of this paper to the adsorption literature.

2. Experimental

2.1 Materials

Deionized water was utilized for preparing all solution preparations. Merck provided the enalapril maleate (CAS 76095-16-4; 492.525 g mol^{-1}; Fig. S1). Inorganic reactants (i.e., HCl, NaOH, and $ZnCl_2$) were furnished by Labsynth with analytical grades and were used as received.

2.2 Activated biochar

The activated biochars were prepared in consecutive steps. First, 100 g of the Bc seeds were milled to a particle diameter lower than 0.25 mm and mixed with zinc chloride solution (100 g of $ZnCl_2$ dissolved in 50 mL of water) to form a homogeneous paste [35]. After drying at 85°C in a conventional furnace for 120 min, the dried paste was put in a stainless reactor in the furnace. Subsequently, the reactor was warmed from room temperature up to 600°C (10°C min^{-1}) using nitrogen gas as purge gas (200 mL min^{-1}), and then the temperature was maintained at this temperature for 30 min. Next, the system was cooled down until the

temperature dropped to 200°C. After cooling, the pyrolyzed material was refluxed with 6 mol L^{-1} HCl at 80°C for 2 h [36]. Subsequently, the material was dried in an oven at 95°C and called BcB-1.0. Another material (BcB-1.5) was similarly prepared using 100.0 Bc and 150 g $ZnCl_2$.

2.3 Biochars characterization

The textural properties of BcB-1.0 and BcB-1.5 biochars were attained employing N_2 adsorption and desorption isotherms utilizing a surface analyzer furnished by Micromeritics, model TriStar 3000. The textural properties (S_{BET}, total pore volume, and pore size distribution) were determined as recommended [37,38].

Fourier-transform infrared spectroscopy (FTIR) spectra were recorded from both activated biochars using an IR Prestige-21Fourier Shimadzu) [39], with KBr pellets. The CHN elemental analysis was acquired using an Agilent analyzer [35].

The hydrophobicity balance (HI) was conducted as previously described [18,20,21].

The thermogravimetric analysis (TGA) analysis of the BcB-1.0 and BcB-1.5 biochars was obtained using TA equipment (model SDT Q600). The analysis was conducted from 20°C to 800°C using nitrogen (10°C min^{-1}) and from 800–1000°C under synthetic air (10°C min^{-1}) [32,33]. The first range from 20 to 800°C was to verify the thermal behavior of the BcB-1.0 and BcB-1.5 under an N_2 atmosphere, and the second range (800–1000°C) was utilized to degrade the carbon matrix, forming residual ashes [32,33].

The point of zero-charge (pH_{pzc}) of BcB-1.0 and BcB-1.5 was measured as previously described [32].

2.4 Adsorption experiments

The batch adsorption experiments employed adsorbent (BcB-1.0 and BcB-1.5) and

161 adsorbate (enalapril) [40-43]. Further details were provided in Supplemental Material.

162 The kinetic and equilibrium data were modeled using nonlinear fitting [44]. The statistical
163 evaluation (Supplemental Material) of these models was performed using the standard
164 deviation of residues (SD), $R^2_{adjusted}$, and Bayesian Information Criterion (BIC) [44,45].

165

166 *2.5. Adsorption kinetics, isotherms, and thermodynamics*

167

168 The kinetic adsorption data were assessed using four nonlinear models such as pseudo-
169 first-order (PFO) [44], pseudo-second-order PSO [44], fractal-like pseudo-first-order (FL-PFO)
170 [46], and fractal-like pseudo-second-order (FL-PSO) ones [46].

171 The isotherm data were explored using the models of Liu [44], Freundlich [44], and
172 Langmuir [44]. Details are shown in Supplemental Material [44,46].

173 In order to explore the influence of temperature and the interactions between BcB-1.0 (or
174 BcB-1.5) and enalapril, thermodynamic studies were conducted from 10°C to 45°C [44,47-49].
175 Details are shown in Supplemental Material.

176

177 *2.6. DFT computational study*

178

179 Atomistic simulations in the framework of the density functional theory (DFT) were
180 performed with the Gaussian16 software package [50], applying the M06-2X exchange-
181 correlation functional [51] and a 6-31G(d) basis set. Geometry optimizations were conducted
182 without symmetry constraints, and frequency calculations followed them to confirm that all
183 structures correspond to energy minima. The interaction energies are calculated as the
184 difference between the overall system energy and the energies for each component. According
185 to the Counterpoise method, they were corrected for the basis set superposition error (BSSE)
186 in all the complexes [52]. The solvent effects (i.e., water) were modeled according to the
187 Polarizable Continuum Model (PCM) [53,54], where the solvent dielectric response is projected

188 on the surface of a cavity of molecular shape where the solute is placed.

189

190 *2.7. Synthetic wastewater*

191

192 Two pharmaceutical-industry wastewater samples with eight pharmaceuticals, two sugars,
193 four organics, and eight inorganic salts were produced (Table S1) [19-21]. The quantities of
194 the chemicals present in the synthetic wastewater are consistent with industrial-
195 pharmaceutical effluents and hospital effluents [19-21].

196

197 ## 3. Results and discussion

198 *3.1 Characterization of BcB-1.0 and BcB-1.5*

199

200 The isotherms of adsorption and desorption of nitrogen for BcB-1.0 and BcB-1.5 carbon
201 materials (Fig. 1) can be classified as type I(b) according to IUPAC [37]. The isotherm type I(b)
202 is compatible with materials exhibiting a mixture of microporous and mesoporous [37] (Fig 1b).
203 The pore size distribution curves of both carbon materials presented a fraction of pores with
204 diameters 1–2 nm (microporous materials) and a fraction of 2 to less than 6 nm (mesopores).
205 The highest nitrogen volumes adsorbed by BcB-1.0 and BcB-1.5 at $p/p°$ = 0.99 were
206 433.4 and 512.4 $cm^3 g^{-1}$, respectively. The total pore volumes were 0.392 (BcB-1.0) and 0.492
207 $cm^3 g^{-1}$ (BcB-1.5). Their Brunauer–Emmett–Teller (BET) surface areas were 1267 (BcB-1.0)
208 and 1520 $m^2 g^{-1}$ (BcB-1.5). These textural characteristics agree with previously prepared
209 activated biochars [32,39]. For example, Cimirro et al. [32] prepared activated biochar from
210 *Pinus elliottii* sawdust and obtained an S_{BET} of 1473 $m^2 g^{-1}$ and TPV of 0.707 $cm^3 g^{-1}$. Dos Reis
211 et al. [39] used bark trees as a carbon source for producing active biochar. They obtained S_{BET}
212 ranging from 98 $m^2 g^{-1}$ (chemically treated with $MgCl_2$) to 2209 $m^2 g^{-1}$ (chemically activated
213 with KOH) and total pore volume ranging from 0.31 (chemically treated with $MgCl_2$) to 1.49

214 $cm^3 g^{-1}$ (chemically activated with KOH). In general, the textural characteristics of the carbon-
215 based material are strongly dependent on carbon sources, types of activation (chemical or
216 physical), heating programs used during pyrolysis, chemical activators (salts employed in
217 impregnation steps), and extraction utilized to remove residual inorganics after pyrolysis steps
218 [32,33,35,39].

219

220 <Fig 1>

221

222 The functional groups on the surface of BcB-1.0 and BcB-1.5 activated biochars were
223 attained using the FTIR technique (Fig 2). The broad band at 3402 cm^{-1} (BcB-1.0) and 3149
224 cm^{-1} (BcB-1.5) belongs to the O–H stretching with intermolecular hydrogen bonding [32,33].
225 Two bands at 2922 and 2852 cm^{-1} for both carbon materials correspond to the asymmetric
226 and symmetric C–H stretching, respectively [35,36]. A band at 1741 cm^{-1} (BcB-1.5) is assigned
227 to C=O of carboxylic acid or aldehyde [40,42]. A band at 1614 cm^{-1} of BcB-1.5 or 1566 cm^{-1} of
228 BcB-1.0 is designated to stretch O=C–O of carboxylates [20,32,33]. Some small bands at 1462
229 cm^{-1} (BcB-1.0), 1460 cm^{-1} (BcB-1.5), and 1400 cm^{-1} (BcB-1.0) are ascribed to C=C of arene
230 rings [20,21]. The bands at 1385 cm^{-1} (BcB-1.0) and 1387 cm^{-1} (BcB-1.5) can be attributed to
231 the C–N chemical bonds of amines or amides that can be overlapped with
232 C-H bending [33,35]. The bands at 1253 cm^{-1} (BcB-1.0) and 1255 cm^{-1} (BcB-1.5) are related
233 to the C–O stretch of ethers or phenols [33,36]. The band at 1150 (BcB-1.0) and 1163 cm^{-1}
234 (BcB-1.5) are denoted to the C–O stretch of alcohols. The bands at 1120 cm^{-1} (BcB-1.0) and
235 1122 cm^{-1} (BcB-1.5) are due to the C–C–O stretch of ester [40,42]. The vibrational bands at
236 877 cm^{-1} and 802 cm^{-1} (BcB-1.0) and 897 cm^{-1} (BcB-1.5) can be designed for C–H out-of-
237 plane bending [32,33].

238

239 < Fig 2>

240

The Boehm titration provides quantitative information regarding the acidic and basic groups on a solid surface [55,56]. The results of the Boehm titration (total acidity and basicity) were obtained for BcB-1.0 (0.5021 and 0.1144 mmol g^{-1}) and BcB-1.5 (0.3937 and 0.09922 mmol g^{-1}, respectively). Furthermore, the number of functional groups on BcB-1.0 was observed to be higher than that on BcB-1.5. As a result, the hydrophobic/hydrophilic (HI) ratio [18,19] of BcB-1.0 and BcB-1.5 was 0.819 and 0.928, respectively. Therefore, HI was calculated as described by equation 1 [18,19].

$$HI = \frac{n - heptane\ vapor\ (mg) \Big/ adsorbent\ mass\ (g)}{water\ vapor\ (mg) \Big/ adsorbent\ mass\ (g)} \quad (1)$$

The values of HI obtained for BcB-1.0 and BcB-1.5 agree with the sum of functional groups present in the carbon-based material. The sum of acid and basic groups of BcB-1.0 and BcB-1.5 was 0.6165 and 0.4929 mmol g^{-1}, respectively. When more functional acidic and basic groups on adsorbent have, the lower value of HI is obtained [20,33]. This is because the acidic and basic groups are polar and tend to uptake water vapor on the solid surface [20,33]. Therefore, BcB-1.5 had 13.31% more hydrophobic behavior when compared to BcB-1.0 due to the lower amount of polar acidic and basic groups [20,33].

Four (BcB-1.0) and five (BcB-1.5) weight losses were viewed in the TGA profiles of the biochar samples (Fig 3). The descriptions of temperature ranges and weight losses can be seen directly in Fig 3. For BcB-1.0, the 1st weight loss can be assigned to adsorbed water losses. The 2nd weight loss can be assigned to water losses in the voids between BC particles and pores and losses of hydroxyl groups of BcB-1.0 biochar [20,32]. The 3rd weight loss is assigned to the decomposition of the carbon matrix when the atmosphere is changed from nitrogen to air [20,32]. Finally, the 4th weight loss is assigned to the finalization of the oxidation of the carbonaceous matrix using oxygen, resulting in inorganic ashes that are left as a residue [35].

<Fig 3>

For BcB-1.5, the 1st stage corresponds to the losses of adsorbed water [20,32]. The second stage is assigned to losses of interstitial water present at the pores or among the carbon particles [20,32]. The 3rd weight loss involves weight losses of releases of hydroxyl and carbonyl groups present on the BcB-1.5 material [20,32]. The 4th stage is assigned to the degradation of carbonaceous bulk when the purge gas is altered from N_2 to synthetic air [20,32]. Finally, the 5th stage corresponds to the complete oxidation of the organic matrix, leading to the formation of inorganic ashes. The ashes contents left in the final residues were 2.27% (BcB-1.0) and 3.11% (BcB-1.5). The higher amount of inorganics left in BcB-1.5 was higher than in BcB-1.0 because the first material utilized 50% more $ZnCl_2$ in the impregnation step. With the HCl leaching out of the inorganics step, the most inorganic matter was removed [35,36], but some residual inorganics could remain in the carbon-based materials [36].

Table 1 presents the elemental analysis (i.e., carbon, hydrogen, and nitrogen) of the BcB-1.0 and BcB-1.5 activated biochars.

<Table 1>

Comparing BcB-1.5 with BcB-1.0, the content of C increased by 10.17%, H content decreased by 49.75%, N content decreased by 48.63%, O content decreased by 29.70%, and ashes content increased by 37.00%. These results show that BcB-1.5 activated biochar had fewer functional groups than BcB-1.0, as discussed above, being BcB-1.5 more hydrophobic than BcB-1.0. Furthermore, the molar ratio C/H of BcB-1.5 was 119.2% higher than that of BcB-1.0, indicating more C atoms for each hydrogen present in the carbonaceous material. This result shows that the biomass formed aromatic condensed rings during the pyrolysis. The higher the ratio C/H is, the more aromatic the structure of the carbon-based material. When the C/H molar ratio decreased, carbon-based material presented a higher content of aliphatics. The molar ratio C/(O + N) of BcB-1.5 was 60.56% higher than that for BcB-1.0. This result shows that BcB-1.5 had fewer functional groups than BcB-1.0, as observed in the Boehm titration.

The pH_{pzc} values of BcB-1.0 and BcB-1.5 biochars were 5.85 and 6.61, respectively (Fig

4). These values showed that BcB-1.0 presented more acidic groups than BcB-1.5. Again, these results match the Bohem titration discussed above and the results in Table 1.

3.2 Preliminary batch contact adsorption experiments.

The influence of initial pH is one of the main factors that should be taken into account for optimizing the parameters in the batch adsorption systems. Fig S2 depicts the pH effect on the enalapril uptake by the BcB-1.0 and BcB-1.5 biochars. At pH 2.0, the enalapril removals were 65.32% (BcB-1.0) and 72.54% (BcB-1.5); these values augmented up to pH 5.1, attaining 75.37% (BcB-1.0) and 85.54% (BcB-1.5). From pH 5.1 up to 10.1, the removal percentage was practically constant for both adsorbents. Making average values from the removal percentages (pH 5.1–10.1), the percentage of removal (%) was 77.52 ± 0.96 (BcB-1.0) and 86.27 ± 0.44 (BcB-1.5). In order to continue this work, the initial pH of enalapril solutions was fixed at 7.0, taking into account that neutral solutions are an adequate medium for the treatment of effluents [1,22,32].

The pHpzc of BcB-1.0 and BcB-1.5 was respectively 5.85 and 6.61. The p*K*a values of enalapril are 3.16, 3.88, and 5.21 (see Figs. S1 and S3). At pH 7.0, the specie D (Fig S3) is the predominant specie of enalapril (98.39%). The specie D contains a carboxylate that is negatively charged. At pH 7.0, both biochars are negatively charged. Therefore, based on these experiments of the effect of initial solutions pH, pH_{pzc} values of the biochar, and p*K*a values of enalapril, it is possible to infer that the mechanism for uptaking the enalapril drug was not electrostatic.

The effect of adsorbent mass on the removal percentage and in the enalapril uptake using both biochars is shown in Fig S4. The behavior of these curves is similar to both biochars. The maximum enalapril removal percentage is practically constant for adsorbent mass >50.0 mg. Conversely, the sorption capacity decreased continuously with an increase in adsorbent mass. This effect can be mathematically expected [57]:

$$q = \frac{\%\ Removal.\ C_0.V}{100.m} \quad (2)$$

In Equation 2, the adsorbent sorption capacity (q) is inversely proportional to the adsorbent mass (m). Therefore, an increase in the adsorbent mass will make the sorption capacity decrease (when considering the adsorbate volume V and initial drug concentration C_o were fixed values). Besides Equation 2, the decrease of sorption capacity with increasing adsorbent mass can be explained using two factors.

- An increase in adsorbent mass using a fixed initial concentration and adsorbate volume will lead to the unsaturation of adsorption sites through the adsorption process;
- The diminution of q can be assigned to the adsorbent particle aggregation for elevated adsorbent masses. This adsorbent aggregation will lead to a diminution of adsorbent surface area and an increase in adsorbate diffusional path length [57].

Also, observing Fig S4, the difference in the removal percentage among 30–50 mg intervals was around 1%. However, the difference in sorption capacities in the 30–50 mg interval was higher than 63% in sorption capacities. In this sense, in this work, the adsorbent mass was fixed at 30.0 mg for continuing this work.

3.3 Adsorption kinetic study

The kinetics for enalapril adsorption on BcB-1.0 and BcB-1.5 was explored, and the kinetic parameters (Table S2) and the kinetic profiles (Fig. 5) were presented. The statistical parameters $R^2_{adj,}$ SD, and BIC values were used to assess the best-fitting of the experimental data. The best-fitted kinetic model will have a R^2_{adj} value closer to 1.00, the lowest SD and BIC values [19-21]. Table S2 shows that the FPSO kinetic model has R^2_{adj} values closer to 1.00, and the minor SD values were obtained for both biochar materials.

The difference in BIC values between pseudo-first-order and fractal-like pseudo-second-order models ranged from 45.23 to 79.39 (BcB-1.0) and 79.66 to 83.13 (BcB-1.5); between

pseudo-second-order and fractal-like pseudo-second-order were 19.62–49.85 (BcB-1.0) and 60.55–62.22 (BcB-1.5); and between fractal-like pseudo-first-order and fractal-like pseudo-second-order were 20.23–54.27 (BcB-1.0) and 58.69–61.70 (BcB-1.5). These BIC differences between PFO and FPSO, PSO and FPSO, and FPFO and FPSO were consistently higher than 10, indicating that the fractal-like pseudo-second-order model was the most suitable kinetic data for describing the uptake of enalapril on both carbon-based adsorbents [32,36,44,45].

<Fig 5>

Considering that different kinetic models have different units for the kinetic constant-rate, it becomes difficult to compare them. On the other hand, the time to attain 50% ($t_{0.5}$) and 95% ($t_{0.95}$) of saturated adsorbent have been successfully employed to compare these different kinetic models [19-21,32,36,44]. Since fractional-like pseudo-second-order was the best-fitted kinetic model, the values $t_{0.5}$ were 1.894–1.881 min (BcB-1.0) and 1.888–1.894 min (BcB-1.5). The values $t_{0.95}$ were 22.22–22.44 min (BcB-1.0) and 20.37–21.00 min (BcB-1.5). The low values of time to attain 50% and 95% of adsorbent saturation [44] indicated that the uptake kinetics of enalapril on both carbon-based adsorbents was fast [44]. In order to continue this research, the time of contact between the adsorbent and adsorbate was set at 40 min ($>t_{0.95}$) to ensure that the contact time is sufficient for attaining equilibrium [44].

3.4 Adsorption isotherm study

The uptake isotherms for enalapril onto BcB-1.0 and BcB-1.5 biochars were conducted at different temperatures of 10–45°C (Table S3). The uptake isotherms of enalapril on both carbon-based materials at 45°C are depicted in Fig 6. The adequacy of the equilibrium models was checked using R^2_{adj}, SD, and BIC values. According to these statistical parameters, the

Liu isotherm was the best-fitted equilibrium model, with R^2_{adj} being 0.9991–0.9999. Also, this model's SD and BIC values were the lowest [22,44]. The difference between the BIC values of the Langmuir model minus those of the model ranged from 38.46 to 251.9 for BcB-1.0. For the BcB-1.5 carbon adsorbent, at 10°C, ΔBIC between the Langmuir and Liu models was 4.514; however, from 20°C to 45°C, the corresponding values ranged from 91.58 to 120.9. The difference in BIC value between Freundlich and Liu ranged from 45.44–261.7 (BcB-1.0) and 110.4–126.1 (BcB-1.5). It is well known that 2< ΔBIC <6, the model with the low value of BIC, tends to be the best-fitted model [44,45]. On the other hand, for ΔBIC >10, the model with the low BIC value is undoubtedly the best-adjusted model [44,45]. Based on the results above for BcB-1.0, indeed, the Liu model is better fitted than the Langmuir and Freudlich model because of ΔBIC >10. The Liu model was the best-fitted for BcB-1.5 from 20–45°C. At 10°C using BcB-1.5 carbon adsorbent, the Liu model tends to be the best-fitted model compared to the Langmuir model [44,45].

There is no regular pattern of Q_{max} values with increasing temperatures for the uptake of enalapril using BcB-1.0 and BcB-1.5. However, at 45°C, the maximum values of Q_{max} (Liu model) were obtained as 347.5 mg g^{-1} (BcB-1.0) and 455.3 mg g^{-1} (BcB-1.0). In contrast, the K_g values regularly decreased with increasing temperatures for both carbon-based materials, indicating that the adsorption process was exothermic for the uptake of enalapril on both biochars [47-49] (Table S3).

<Fig 6>

No reported study deals with removing enalapril as an adsorbate, so these sorption capacities were considered high compared to other pharmaceuticals. For example, Cunha et al. [21] obtained Q_{max} values (Liu isotherm) ranging from 442.2 to 717.2 mg g^{-1} to uptake captopril using *Butia catarinensis* activated carbon. Dos Reis et al. [39], using bark-activated biochars, obtained Q_{max} values (Liu isotherm) ranging from 321.2 to 752.7 mg g^{-1} for the uptake of acetaminophen. Using magnetic biochar, Thue et al. [20] obtained Q_{max} values (Liu isotherm) ranging from 159.2 to 199.3 mg g^{-1} to uptake nicotinamide and Q_{max} values ranging from 301.0

398 to 335.4 mg g^{-1} for the uptake of propranolol.

399

400 *3.5 Adsorption thermodynamics and mechanism*

401

402 The thermodynamic parameters of adsorption Δ*H*° and Δ*S*° were attained employing the
403 nonlinear van't Hoff plot [49] (see Fig S5). The K_e^0 values [47,48] were acquired utilizing the
404 values of K_g from the Liu isotherm at 283–318 K (see Supplementary Material and Table S4).
405 The standard Gibb's energy change (Δ*G*°) values were all negative for 283–318 K (Table S4),
406 indicating favorable and spontaneous adsorption processes for both carbon-based
407 adsorbents. The values Δ*H*° were –35.46 (BcB-1.0) and –35.18 kJ mol^{-1} (BcB-1.5). These
408 values of Δ*H*° are in agreement with a physical adsorption process [58,59]. Hydrogen bonds
409 have Δ*H*° values ranging from 25 to 60 kJ mol^{-1} [58,59], which matches the value of Δ*H*° of
410 adsorption. Therefore, it could be assumed that the uptake of enalapril onto BcB-1.0 and BcB-
411 1.5 activated biochars is governed by physical adsorption.

412 Considering the enalapril physicochemical properties and the chemical structure of
413 adsorbate (enalapril) and activated biochars, interaction mechanisms between the adsorbent
414 and adsorbate took place by the donor–acceptor interactions (*n*–π interaction) that takes place
415 between arene rings in the biochar that work as an electron acceptor and the carboxylate
416 groups of enalapril. In addition, the O of carbonyl groups and the N of the secondary amine
417 and proline groups on the enalapril can work as an electron acceptor [21,33].

418 Another remarkable interaction is the hydrogen bonding of –OH groups available on
419 biochars with the O (carbonyl and carboxylate) and N atoms (secondary amine and proline) of
420 the enalapril, at pH 7.0 (see the structure D in Fig S3) [21]. In addition, C-H's van der Waals
421 interaction, known as hydrophobic interactions, occurred [21,33]. Furthermore, considering the
422 BcB-1.0 and BcB-1.5 textural properties, the pore-filling mechanism should also take place as
423 the primary contributor to the overall uptake of enalapril. The diagram in Fig 7 presented
424 mechanisms suggested for adsorbing enalapril onto both biochars. In order to identify more

accurately which kind of interaction mainly drive the adsorption of enalapril, DFT calculations were conducted.

<Fig 7>.

3.6. DFT computational study

The interaction between enalapril and a graphitic domain of a biochar pore, modeled by a circumcircumcoronene molecule ($C_{96}H_{24}$), has been theoretically explored by the DFT calculations. Four configurations for enalapril toward the graphitic domain differed in the main adsorbate segments interacting with the biochar pore (Figure 8). Among these adsorption configurations, the most stable one, depicted by interaction energy of –88.7 kJ mol^{-1}, implies a face-to-face π–π stacking interaction involving the enalapril phenyl segment and an aromatic ring of $C_{96}H_{24}$, as well as London dispersion (van der Waals interaction) arising from the proximity of ethoxy/pyrrolidine to $C_{96}H_{24}$ carbon atoms, with interatomic distances of 3.31 Å for the former and 3.60 Å /3.48 Å for the latter (Figure 8a). Remarkably, the magnitude of this interaction energy corresponds to a noncovalent assembly, in line with the adsorption process herein described.

Slightly lower interaction energies are found for the second adsorption mode, where the ethoxy contribution to the noncovalent interplay is precluded (Figure 8b), and the third one, where a tilted face-to-edge π–π stacking occurs (Figure 8c) with an inter-ring distance of 3.57 Å, larger than the face-to-face one observed in the most stable case. The obtained interaction energies are –75.3 kJ mol^{-1} and –67.4 kJ mol^{-1}, respectively, suggesting a more relevant role played by the phenyl ring compared to ethoxy in the adsorbate anchoring to the biochar pore. Finally, in the last enalapril configuration, the π–π stacking is precluded (Figure 8d), enabling only the ethoxy and pyrrolidine segments to contact $C_{96}H_{24}$, resulting in the lowest interaction energy of the considered series, i.e., –28.0 kJ mol^{-1}, confirming the pivotal role of phenyl in the enalapril adsorption toward a graphitic domain of biochar.

<Fig 8>

3.7. Adsorption under synthetic effluent conditions

Based on the batch contact adsorption studies and also the remarkable textural characteristics of BcB-1.0 and BcB-1.5 activated biochars, it is supposed that both materials can be applied for wastewater treatment of pharmaceutical industrial effluents. Therefore, 2 synthetic wastewaters (Table S1) were used for evaluating the accomplishment of BcB-1.0 and BcB-1.5 material for the uptake of several medicines mixed with different chemicals available in industrial effluents [19,22] (Fig 9 and Table S1).

The molecular absorption spectra of two types of wastewaters were utilized to evaluate the total quantity of all substances uptaken (Fig. 9). The UV-Vis spectra were recorded from 190 to 500 nm before and after the batch-contact adsorption procedure with both biochars. The overall removal percentage of all the components in both synthetic effluents was obtained by integrating the area under the absorption band, as previously described [19-22].

After the complete adsorption, it was attained a removal percentage of 98.66% (effluent A) and 98.09% (effluent B) using BcB-1.0 and 99.06% (effluent A) and 98.59% (effluent B) using BcB-1.5 activated biochars. It is essential to focus on the fact that both carbon adsorbent materials presented elevated uptake of overall organic compounds, even when the chemical quantities were doubled. These observations indicate that both carbon-based materials can be employed for actual wastewater treatment in the pharmaceutical industry.

<Fig 9>

4. Conclusions

The BcB-1.0 and BcB-1.5 activated biochar adsorbed enalapril maleate efficiently from aqueous wastewater. Both biochars were chemically activated, forming biochar with outstanding textural properties such as high surface areas 1267 (BcB-1.0) and 1520 $m^2\ g^{-1}$

(BcB-1.5) and high total pore volumes 0.392 (BcB-1.0) and 0.492 cm^3 g^{-1} (BcB-1.5). Based on the Bohem titration, it was obtained the total acidity of 0.5021 (BcB-1.0) and 0.3937 mmol g^{-1} (BcB-1.5), and the total basicity obtained was 0.1144 (BcB-1.0), and 0.09922 mmol g^{-1} (BcB-1.5). The hydrophobic/hydrophilic ratio (HI) of BcB-1.0 was 0.819, and that of BcB-1.5 was 0.928. The values of HI obtained for BcB-1.0 and BcB-1.5 are in agreement with the sum of functional groups present in the carbon-based material. The FTIR analysis showed that both biochars presented the OH, COOH, arene rings, phenol, esters, and groups that could interact well with enalapril maleate.

The kinetic studies showed that the fractal-like pseudo-second-order was the most suitable kinetic model for describing the uptake of enalapril on both carbon-based adsorbents. The isotherm data were better fitted to the nonlinear Liu model (10–45°C). At 45°C, the maximum values of Q_{max} (Liu model) were obtained, being 347.5 (BcB-1.0) and 455.3 mg g^{-1} (BcB-1.0). The thermodynamic adsorption studies were conducted using the equilibrium constant obtained from the Liu isotherm from 283–318 K. The standard Gibb's energy change ($\Delta G°$) values were all negative for this temperature range, indicating favorable and spontaneous adsorption processes for both carbon-based adsorbents. The $\Delta H°$ were –35.46 (BcB-1.0) and –35.18 kJ mol^{-1} (BcB-1.5). These values of $\Delta H°$ agree with a physical adsorption process confirmed by DFT calculations. Both activated biochars were used for treating simulated pharmaceutical industry wastewater. It attained an overall removal percentage of up to 99.06%.

Acknowledgments

The authors thank CAPES (001), CNPq (303.612/2021-5 and 402.450/2021-3), and FINEP (044/21/IAP 1942/FAURGS 8638) from Brazil for financing part of this research. Finally, the authors are also grateful to the Researchers Supporting Project number (RSP2023R8), King Saud University, Riyadh, Saudi Arabia, for the financial support. Also, the authors are grateful to the Nanoscience and Nanotechnology Center (CNANO-UFRGS) of the Federal University

of Rio Grande do Sul (UFRGS) for conducting several analyses. The authors are also grateful to ChemAxon for giving us an academic research license for the Marvin Sketch software, Version 23.7.0 (http://www.chemaxon.com), 2023, used for molecule physical-chemical properties.

References

[1] C.A. Sophia, E.C. Lima, Removal of emerging contaminants from the environment by adsorption. Ecotoxicol. Environ. Saf. 150 (2018) 1–17.

[2] B. Mishra, A. Mukherjee, A. Mullick, V.M. Bhandari, S. Moulik. Design of hydrodynamic cavitation assisted intensified tertiary treatment unit for effective degradation of organic micropollutants in pharmaceutical industrial effluent: A Case study with triclosan. J. Water Proc. Eng. 49 (2022) 103132. Doi:10.1016/j.jwpe.2022.103132.

[3] M. Gustavsson, S. Molander, T. Backhaus, E. Kristiansson. Estimating the release of chemical substances from consumer products, textiles, and pharmaceuticals to wastewater. Chemosphere 287 (2022) 131854. Doi:10.1016/j.chemosphere.2021.131854.

[4] NORMAN. The network of reference laboratories, research centres, and related organisations for monitoring of emerging environmental substances. www.norman-network.net. It was accessed on January 16th, 2023.

[5] V.K. Parida, D. Saidulu, A. Majumder, A. Srivastava, B. Gupta, A.K. Gupta. Emerging contaminants in wastewater: A critical review on occurrence, existing legislation, risk assessment, and sustainable treatment alternatives. J. Environ. Chem. Eng. 9 (2021), 105966. Doi:10.1016/j.jece.2021.105966.

[6] P.A. Muniozguren, E.A. Serna-Galvis, M. Bussemaker, R.A. Torres-Palma, J. Lee. A review on pharmaceuticals removal from waters by single and combined biological,

533 membrane filtration, and ultrasound systems. Ultrason. Sonochem. 76 (2021) 105656.
534 Doi:10.1016/j.ultsonch.2021.105656.
535 [7] P. Tripathy, O. Prakash, A. Sharma, D. Panchal. Chapter 7 - Antibiotics in wastewater: a
536 perspective of biological treatment processes. Degradation of Antibiotics and Antibiotic-
537 Resistant Bacteria from Various Sources. Developments in Microbiology. P. SINGH, M.
538 SILLANPA (eds). Elsevier, 2023, Pages 159-177. Doi:10.1016/B978-0-323-99866-
539 6.00004-0.
540 [8] C. Ding, Q. Zhu, B. Yang, E. Petropoulos, L. Xue, Y. Feng, S. He, L. Yang. Efficient
541 photocatalysis of tetracycline hydrochloride (TC-HCl) from pharmaceutical wastewater
542 using AgCl/ZnO/g-C_3N_4 composite under visible light: Process and mechanisms. J.
543 Environ. Sci. 126 (2023) 249-262. Doi:10.1016/j.jes.2022.02.032.
544 [9] N.S. Abbood, N.S. Ali, E.H. Khader, H.Sh. Majdi, T.M. Albayati, N.M.C. Saady.
545 Photocatalytic degradation of cefotaxime pharmaceutical compounds onto a modified
546 nanocatalyst. Res. Chem. Intermed. 49 (2023) 43-56. Doi:10.1007/s11164-022-04879-3.
547 [10] A. Della-Flora, M.L. Wilde, P.S. Thue, D.R. Lima, E.C. Lima, C. Sirtori. Combination of
548 solar photo-Fenton and adsorption process for removal of the anticancer drug Flutamide
549 and its transformation products from hospital wastewater. J. Hazard. Mater.,396 (2020),
550 122699. DOI:10.1016/j.jhazmat.2020.122699.
551 [11] A. Della-Flora, M.l. Wilde, I.D.F. Pinto, E.C. Lima, C. Sirtori, Degradation of the anticancer
552 drug flutamide by solar photo-Fenton treatment at near-neutral pH: Identification of
553 transformation products and in silico (Q)SAR risk assessment. Environ. Res., 183 (2020)
554 109223. Doi:10.1016/j.envres.2020.109223.
555 [12] M. Bosio, B.M. de Souza-Chaves, E.M. Saggioro, J.P. Bassin, M.W.C. Dezotti, M.E.
556 Quinta-Ferreira, R.M. Quinta-Ferreira. Electrochemical degradation of psychotropic
557 pharmaceutical compounds from municipal wastewater and neurotoxicity evaluations.
558 Environ. Sci. Pollut. Res. 28 (2021) 23958–23974. Doi:10.1007/s11356-020-12133-9.
559 [13] J.D. García-Espinoza, P.M. Nacheva. Degradation of pharmaceutical compounds in

560 water by oxygenated electrochemical oxidation: Parametric optimization, kinetic studies,
561 and toxicity assessment. Sci. Total Environ. 691 (2019) 417-429.
562 Doi:10.1016/j.scitotenv.2019.07.118.
563 [14] Y. Wang, H. Huang, X. Wei. Influence of wastewater pre-coagulation on adsorptive
564 filtration of pharmaceutical and personal care products by carbon nanotube membranes.
565 Chem. Eng. J. 333 (2018) 66-75. Doi:10.1016/j.cej.2017.09.149.
566 [15] M. Klatt, F. Beyer, J. Einfeldt. Hospital wastewater treatment and the role of membrane
567 filtration – removal of micropollutants and pathogens: A review. Water Sci Technol 86
568 (2022) 2213–2232. Doi:10.2166/wst.2022.321.
569 [16] F. Ghanbari, A. Hassani, S. Wacławek, Z. Wang, G. Matyszczak, K.Y.A. Lin, M.
570 Dolatabadi. Insights into paracetamol degradation in aqueous solutions by ultrasound-
571 assisted heterogeneous electro-Fenton process: Key operating parameters,
572 mineralization, and toxicity assessment. Sep. Purif. Technol. 266 (2021) 118533.
573 Doi:10.1016/j.seppur.2021.118533.
574 [17] A.L. Camargo-Perea, E.A. Serna-Galvis, J. Lee, R.A. Torres-Palma. Understanding the
575 effects of mineral water matrix on the degradation of several pharmaceuticals by
576 ultrasound: Influence of chemical structure and concentration of the pollutants. Ultrason.
577 Sonochem. 73 (2021) 105500. Doi:10.1016/j.ultsonch.2021.105500.
578 [18] G.S. dos Reis, C.H. Sampaio, E.C. Lima, M. Wilhelm. Preparation of novel adsorbents
579 based on combinations of polysiloxanes and sewage sludge to remove pharmaceuticals
580 from aqueous solutions, Colloids Surf. A, 497 (2016) 304–315.
581 [19] M.González-Hourcade, G.S. dos Reis, A. Grimm, V.M. Dinh, E.C. Lima, S.H. Larsson,
582 F.G. Gentili. Microalgae biomass as a sustainable precursor to produce nitrogen-doped
583 biochar for efficient removal of emerging pollutants from aqueous media. J. Clean. Prod.
584 348 (2022) 131280. Doi:10.1016/j.jclepro.2022.131280.
585 [20] P.S. Thue, C.S. Umpierres, E.C. Lima, D.R. Lima, F.M. Machado, G.S. dos Reis, R.S. da
586 Silva, F.A. Pavan, H.N. Tran. Single-step pyrolysis for producing magnetic activated

carbon from tucumã (*Astrocaryum aculeatum*) seed and nickel(II) chloride and zinc(II) chloride. Application for removal of Nicotinamide and Propanolol. J. Hazard. Mater., 398 (2020) 122903. Doi:10.1016/j.jhazmat.2020.122903.

[21] M.R. Cunha, E.C. Lima, D.R. Lima, R.S. da Silva, P.S. Thue, M.K. Seliem, F. Sher, G.S. dos Reis, S.H. Larsson. Removal of captopril pharmaceutical from synthetic pharmaceutical-industry wastewaters: use of activated carbon derived from *Butia catarinensis*. J. Environ. Chem. Eng. 8 (2020) 104506. Doi: 10.1016/j.jece.2020.104506.

[22] D.F. Caicedo, G.S. dos Reis, E.C. Lima, I.A.S. de Brum, P.S. Thue, B.G. Cazacliu, D.R. Lima, A.H. dos Santos, G.L. Dotto. Efficient adsorbent based on construction and demolition wastes functionalized with 3-aminopropyltriethoxysilane (APTES) for the removal of ciprofloxacin from hospital synthetic effluents. Journal of Environmental Chemical Engineering, 8 (2020), 103875. Doi:/10.1016/j.jece.2020.103875.

[23] E.H. M. Cavalcante, I.C. M. Candido, H.P. de Oliveira, K.B. Silveira, T.V. S. Álvares, E.C. Lima, M. Thyrel, S.H. Larsson, G.S. dos Reis. 3-Aminopropyl-triethoxysilane-Functionalized Tannin-Rich Grape Biomass for the Adsorption of Methyl Orange Dye: Synthesis, Characterization, and the Adsorption Mechanism. ACS Omega 2022, 7, 22, 18997–19009. Doi:10.1021/acsomega.2c02101.

[24] Q. Wu, Y. Zhang, H. Liu, H. Liu, J. Tao, M.H. Cui, Z. Zheng, D. Wen, X. Zhan. FexN produced in pharmaceutical sludge biochar by endogenous Fe and exogenous N doping to enhance peroxymonosulfate activation for levofloxacin degradation. Water Res. 224 (2022) 119022. Doi:10.1016/j.watres.2022.119022.

[25] A. Della-Flora, D. Scunderlick, M.L. Wilde, A.A. Gomes, E.C. Lima, C. Sirtori. *In silico* environmental risk assessment of fate and effects of pharmaceuticals and their TPs generated and treated by coupling tertiary processes in hospital wastewater. Environ. Sci.: Water Res. Technol., 9 (2023) 274-284. DOI: 10.1039/d2ew00518b.

[26] V. Vinayagam, S. Murugan, R. Kumaresan, M. Narayanan, M. Sillanp, D.V.N. Vo, O.S. Kushwaha, P. Jenis, P. Potdar, S. Gadiya. Sustainable adsorbents for the removal of

614 pharmaceuticals from wastewater: A review. Chemosphere 300 (2022) 134597.
615 Doi:10.1016/j.chemosphere.2022.134597.
616 [27] D.R. Lima, E.C. Lima, P.S. Thue, S.L.P. Dias,F. M. Machado, M.K. Seliem, F. Sher, G.
617 S. dos Reis, M.R. Saeb, J. Rinklebe. Comparison of acidic leaching using a conventional
618 and ultrasound-assisted method for preparation of magnetic-activated biochar.
619 J. Environ. Chem. Eng. 9 (2021) 105865. Doi:10.1016/j.jece.2021.105865.
620 [28] Enalapril- Medline plus. https://medlineplus.gov/druginfo/meds/a686022.html. Web site
621 visited on January 24th, 2023.
622 [29] M. Valilshchykov, V. Babalyan, T. Markina, M. Kumetchko, L. Boiko, S. Romaev. The
623 Enalapril Use in Arterial Hypertension Stimulates The Reparative Processes in Fractures
624 of The Proximal Femur. Indones Biomed J. 14 (2022) 36-44. DOI:
625 10.18585/inabj.v14i1.1736.
626 [30] Brazillian Popular Pharmacy Program. https://consultaremedios.com.br/farmacia-
627 popular. It was accessed on January 24th, 2023.
628 [31] B. Lalović, T, Đurkić, M. Vukčević, I. Janković-Častvan, A. Kalijadis, Z. Laušević, M.
629 Laušević. Solid-phase extraction of multi-class pharmaceuticals from environmental
630 water samples onto modified multi-walled carbon nanotubes followed by LC-MS/MS.
631 Environ. Sci. Pollut. Res. 24 (2017) 20784-20793. DOI 10.1007/s11356-017-9748-0.
632 [32] N.F.G.M. Cimirro, E.C. Lima, M.R. Cunha, P.S. Thue, A. Grimm, G.S. dos Reis, N.
633 Rabiee, M.R. Saeb, F. Keivanimehr, S. Habibzadeh. Removal of diphenols using pine
634 biochar. Kinetics, equilibrium, thermodynamics, and mechanism of uptake. J. Mol. Liq.
635 364 (2022) 119979. Doi:10.1016/j.molliq.2022.119979.
636 [33] A.B. Leite, C. Saucier, E.C. Lima, G.S. dos Reis, C.S. Umpierres, B.L. Mello, M.
637 Shirmardi, S.L.P. Dias, C.H. Sampaio. Activated carbons from avocado seed:
638 Optimization and application for removal of several emerging organic compounds,
639 Environ. Sci. Pollut. Res. 25 (2018) 7647–7661. Doi:10.1007/s11356-017-1105-9.
640 [34] W.P.A. Dias, P.S.N. Lopes, R.S. Fonseca, L.M. Ribeiro, A.P. Gonçalves, B.A.P. Ribeiro.

Reproductive biology *of Butia capitata* (Arecaceae) under cultivation - indicators for the domestication of a threatened fruit tree. Scientia Horticulturae 304 (2022) 111297. Doi:10.1016/j.scienta.2022.111297.

[35] P.S. Thue, E.C. Lima, J.M. Sieliechi, C. Saucier, S.L.P. Dias, J.C.P. Vaghetti, F.S. Rodembusch, F.A. Pavan. Effects of first–row transition metals and impregnation ratios on the physicochemical properties of microwave-assisted activated carbons from wood biomass. J. Colloid Interface Sci. 486 (2017) 163-175. Doi:10.1016/j.jcis.2016.09.0707.

[36] A.J.B. Leite, A.C. Sophia, P.S. Thue, G.S. dos Reis, S.L.P. Dias, E.C. Lima, J.C.P. Vaghetti, F.A. Pavan, W.S. de Alencar. Activated carbon from avocado seeds for the removal of phenolic compounds from aqueous solutions. Desalin. Water Treat. 71 (2017) 168–181. Doi: 10.5004/dwt.2017.20540.

[37] M. Thommes, K. Kaneko, A.V. Neimark, J.P. Olivier, F. Rodriguez-Reinoso, J. Rouquerol, K.S.W. Sing. Physisorption of gases, with special reference to the evaluation of the surface area and pore size distribution (IUPAC Technical Report). Pure Appl. Chem. 87 (2015) 1051–1069.

[38] J. Jagiello, M. Thommes. Comparison of DFT characterisation methods based on N_2, Ar, CO_2, and H_2 adsorption applied to carbons with various pore size distributions, Carbon, 42 (2004) 1227-1232.

[39] G.S. dos Reis, M. Guy, M. Jebrane, E.C. Lima, M. Thyrel, G.L. Dotto, S.H. Larsson. A comparative study of chemical treatment by $MgCl_2$, $ZnSO_4$, $ZnCl_2$, and KOH on physicochemical properties and acetaminophen adsorption performance of biobased porous materials from tree bark residues. Colloids Surf. A 642 (2022) 128626. Doi:10.1016/j.colsurfa.2022.128626.

[40] N.T. Abdel-Ghani, A.K. Hegazy, G.A. El-Chaghaby, E.C. Lima, Factorial experimental design for biosorption of iron and zinc using Typha domingensis phytomass. Desalination, 249 (2009) 343-347. doi:10.1016/j.desal.2009.02.065.

[41] R.A. Jacques, R. Bernardi, M. Caovila, E.C. Lima, F.A. Pavan, J.C. P. Vaghetti, C. Airoldi.

668 Removal of Cu(II), Fe(III), and Cr(III) from Aqueous Solutions by Aniline Grafted Silica
669 Gel. Sep. Sci. Technol., 42 (2007) 591-609. DOI: 10.1080/01496390601069952.
670 [42] J.C.P. Vaghetti, E.C. Lima, B. Royer, N.F. Cardoso, B. Martins, T. Calvete. Pecan
671 Nutshell as Biosorbent to Remove Toxic Metals from Aqueous Solution. Sep. Sci.
672 Technol., 44 (2009) 615-644. DOI: 10.1080/01496390802634331.
673 [43] L.T. Arenas, E.C. Lima, A.A. dos Santos Jr., J.C.P. Vaghetti, T.M.H. Costa, E.V.
674 Benvenutti. Use of statistical design of experiments to evaluate the sorption capacity of
675 1,4-diazoniabicycle[2.2.2]octane/silica chloride for Cr(VI) adsorption. Colloids Surf. A 297
676 (2007) 240-248. doi:10.1016/j.colsurfa.2006.10.050.
677 [44] E.C. Lima, M.H. Dehghani, A. Guleria, F. Sher, R.R. Karri, G.L. Dotto, H.N. Tran,
678 CHAPTER 3 - Adsorption: Fundamental aspects and applications of adsorption for
679 effluent treatment, in: M. Hadi Dehghani, R. Karri, E. Lima (Eds.), Green Technol.
680 Defluoridation Water, Elsevier, 2021: pp. 41–88. Doi: 10.1016/B978-0-323-85768-
681 0.00004-X.
682 [45] E.C. Lima, F. Sher, A. Guleria, M.R. Saeb, I. Anastopoulos, H.N. Tran, A. Hosseini-
683 Bandegharaei. Is one performing the treatment data of adsorption kinetics correctly? J.
684 Environ. Chem. Eng. 9 (2021) 104813. Doi:10.1016/j.jece.2020.104813.
685 [46] M. Haerifar, S. Azizian. Fractal-Like Kinetics for Adsorption on Heterogeneous Solid
686 Surfaces. J. Phys. Chem. C 118 (2014), 1129-1134. Doi:10.1021/jp4110882.
687 [47] E.C. Lima, A. Hosseini-Bandegharaei, J.C. Moreno-Piraján, I. Anastopoulos. A critical
688 review of the estimation of the thermodynamic parameters on adsorption equilibria.
689 Wrong use of equilibrium constant in the Van't Hoof equation for calculation of
690 thermodynamic parameters of adsorption, J. Mol. Liq., 273 (2019) 425-434.
691 Doi:10.1016/j.molliq.2018.10.048.
692 [48] E.C. Lima, A. Hosseini-Bandegharaei, I. Anastopoulos. Response to "Some remarks on
693 a critical review of the estimation of the thermodynamic parameters on adsorption
694 equilibria. Wrong use of equilibrium constant in the van't Hoff equation for calculation of

thermodynamic parameters of adsorption - Journal of Molecular Liquids 273 (2019) 425–434". Journal of Molecular Liquids, 280 (2019) 298-300. Doi:10.1016/j.molliq.2019.01.160.

[49] E.C. Lima, A.A. Gomes, H.N. Tran, Comparison of the nonlinear and linear forms of the van't Hoff equation for calculation of adsorption thermodynamic parameters (ΔS° and ΔH°). J Mol Liq 311 (2020) 113315. Doi:10.1016/j.molliq.2020.113315.

[50] M. J. Frisch, G. W. Trucks, H. B. Schlegel, G. E. Scuseria, M. A. Robb, J. R. Cheeseman, G. Scalmani, V. Barone, G. A. Petersson, H. Nakatsuji, X. Li, M. Caricato, A. V. Marenich, J. Bloino, B. G. Janesko, R. Gomperts, B. Mennucci, H. P. Hratchian, J. V. Ortiz, A. F. Izmaylov, J. L. Sonnenberg, D. Williams-Young, F. Ding, F. Lipparini, F. Egidi, J. Goings, B. Peng, A. Petrone, T. Henderson, D. Ranasinghe, V. G. Zakrzewski, J. Gao, N. Rega, G. Zheng, W. Liang, M. Hada, M. Ehara, K. Toyota, R. Fukuda, J. Hasegawa, M. Ishida, T. Nakajima, Y. Honda, O. Kitao, H. Nakai, T. Vreven, K. Throssell, J. A. Montgomery, Jr., J. E. Peralta, F. Ogliaro, M. J. Bearpark, J. J. Heyd, E. N. Brothers, K. N. Kudin, V. N. Staroverov, T. A. Keith, R. Kobayashi, J. Normand, K. Raghavachari, A. P. Rendell, J. C. Burant, S. S. Iyengar, J. Tomasi, M. Cossi, J. M. Millam, M. Klene, C. Adamo, R. Cammi, J. W. Ochterski, R. L. Martin, K. Morokuma, O. Farkas, J. B. Foresman, and D. J. Fox, Gaussian, Inc., Wallingford CT, 2016.

[51] Y. Zhao, D.G. Truhlar. The M06 suite of density functionals for main group thermochemistry, thermochemical kinetics, noncovalent interactions, excited states, and transition elements: two new functionals and systematic testing of four M06-class functionals and 12 other functionals. Theoretical Chemistry Accounts volume 120 (2008) 215–241. DOI 10.1007/s00214-007-0310-x.

[52] S.F. Boys, F. Bernardi. The calculation of small molecular interactions by the differences of separate total energies. Some procedures with reduced errors, Molecular Physics, 19 (1970) 553-566, DOI: 10.1080/00268977000101561.

[53] B. Mennucci, Polarizable continuum model. Wiley Interdisciplinary Reviews:

722 Computational Molecular Science, 2(2012), 386–404. doi:10.1002/wcms.1086.
723 [54] B. Mennucci, J. Tomasi, R. Cammi, J. R. Cheeseman, M. J. Frisch, F. J. Devlin, S.
724 Gabriel, P. J. Stephens. Polarizable Continuum Model (PCM) Calculations of Solvent
725 Effects on Optical Rotations of Chiral Molecules. J. Phys. Chem. A 106 (2002), 6102-
726 6113. DOI: 10.1021/jp020124t.
727 [55] Goertzen, S.L., Theriault, K.D., Oickle A.M., Tarasuk, A.C., Andreas, H.A.,
728 Standardisation of the Boehm titration. Part I. CO_2 expulsion and endpoint determination.
729 Carbon 48 (2010) 1252–1261.
730 [56] Oickle, A.M., Goertzen, S.L, Hopper, K.R, Abdalla, Y.O., Andreas, H.A., Standardisation
731 of the Boehm titration: Part II. Method of agitation, the effect of filtering, and dilute titrant.
732 Carbon 48 (2010) 3313-3322.
733 [57] J.S. Lazarotto, K.B. Martinello, J. Georgin, D.S.P. Franco, M.S. Netto, D.G.A. Piccilli,
734 L.F.O. Silva E.C. Lima, G.L. Dotto. Preparation of activated carbon from the residues of
735 the mushroom (Agaricus bisporus) production chain for the adsorption of the 2,4-
736 dichlorophenoxyacetic herbicide. J. Environ. Chem. Eng. 9 (2021) 106843.
737 Doi:10.1016/j.jece.2021.106843.
738 [58] R. Chang, J.W. Thoman-Jr, Chapter 17- Intermolecular forces, in "Physical Chemistry for
739 Chemical Sciences," University Science Books, 779-808, (2014).
740 [59] P. Lipkowski, A. Koll, A. Karpfen, P. Wolschann, An approach to estimate the energy of
741 the intramolecular hydrogen bond, Chemical Physics Letters, 10 (2002) 256-263.
742 Doi:10.1016/S0009-2614(02)00830-8.
743
744

745 # List of Tables

746

747 Table 1. Elemental analysis, molar ratio, and HI for BcB-1.0 and BcB-1.5

Sample	Weight ratio				%ash	Molar ratio		HI	pH_{pzc}
	%C	%H	%N	%O		C/H	C/(N+O)		
BcB-1.0	72.56	1.99	1.83	21.35	2.27	3.06	4.12	0.819	5.85
BcB-1.5	79.94	1.00	0.94	15.01	3.11	6.71	6.62	0.929	6.61

748

749

List of Figures

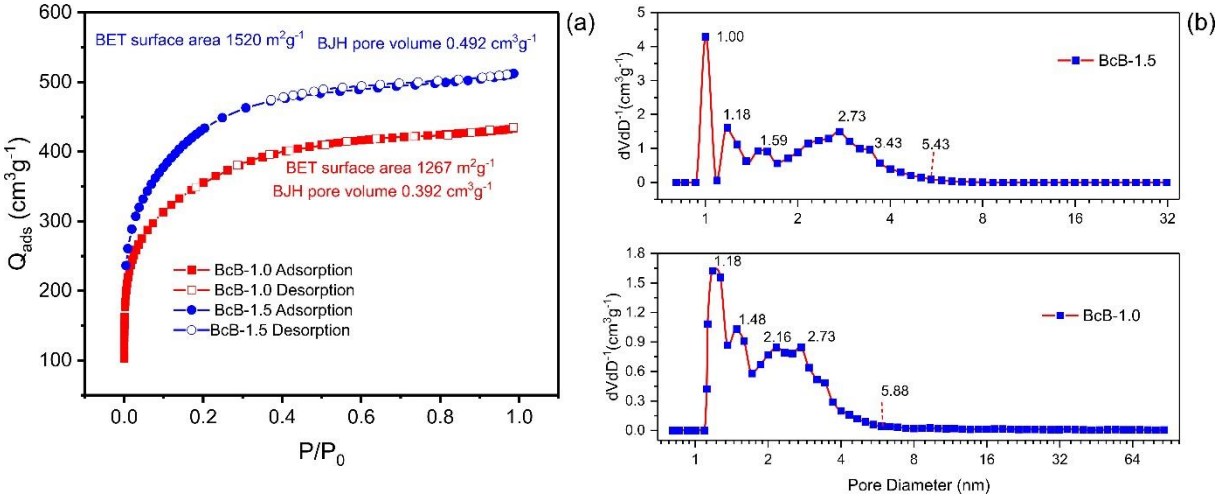

Fig 1. Textural characteristics of BcB-1.0 and BcB-1.5 activated biochars. (a)- N_2 isotherm. (b) pore size distribution.

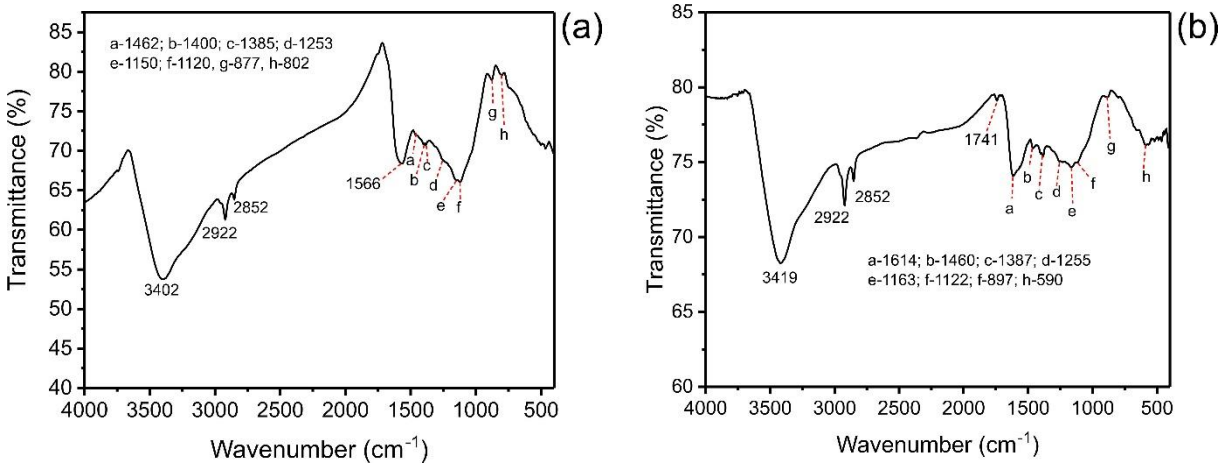

Fig 2. Vibrational spectra of (a) BcB-1.0 and (b) BcB-1.5 activated biochars.

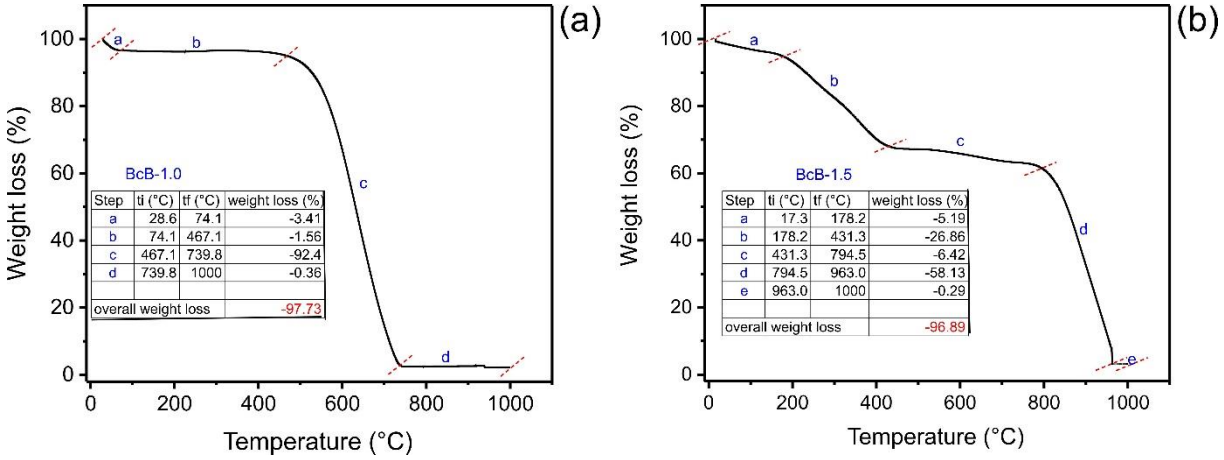

Fig 3. Thermogravimetric analysis of (a) BcB-1.0 and (b) BcB-1.5 biochars.

766

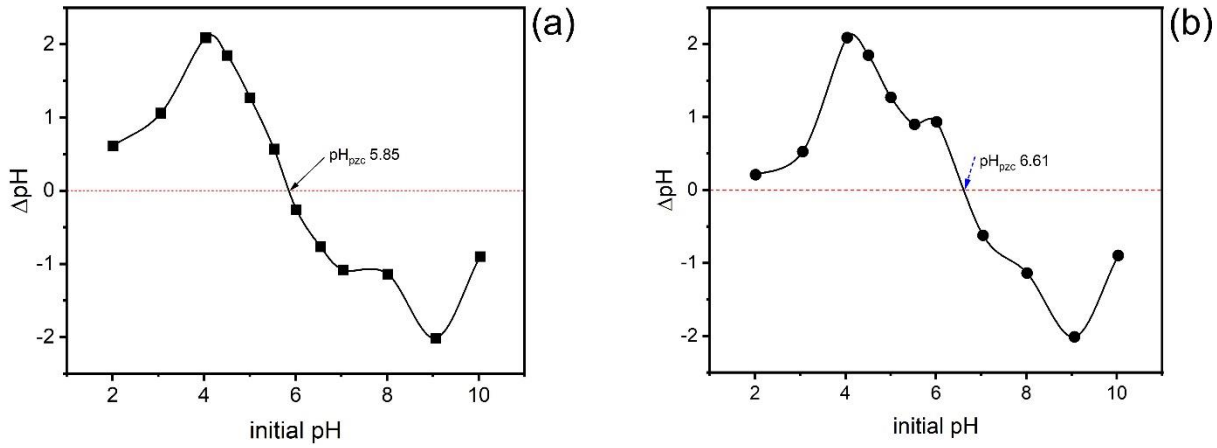

767

768 **Fig 4**. pHpzc of (a) BcB-1.0 and (b) BcB-1.5 activated biochars.

769

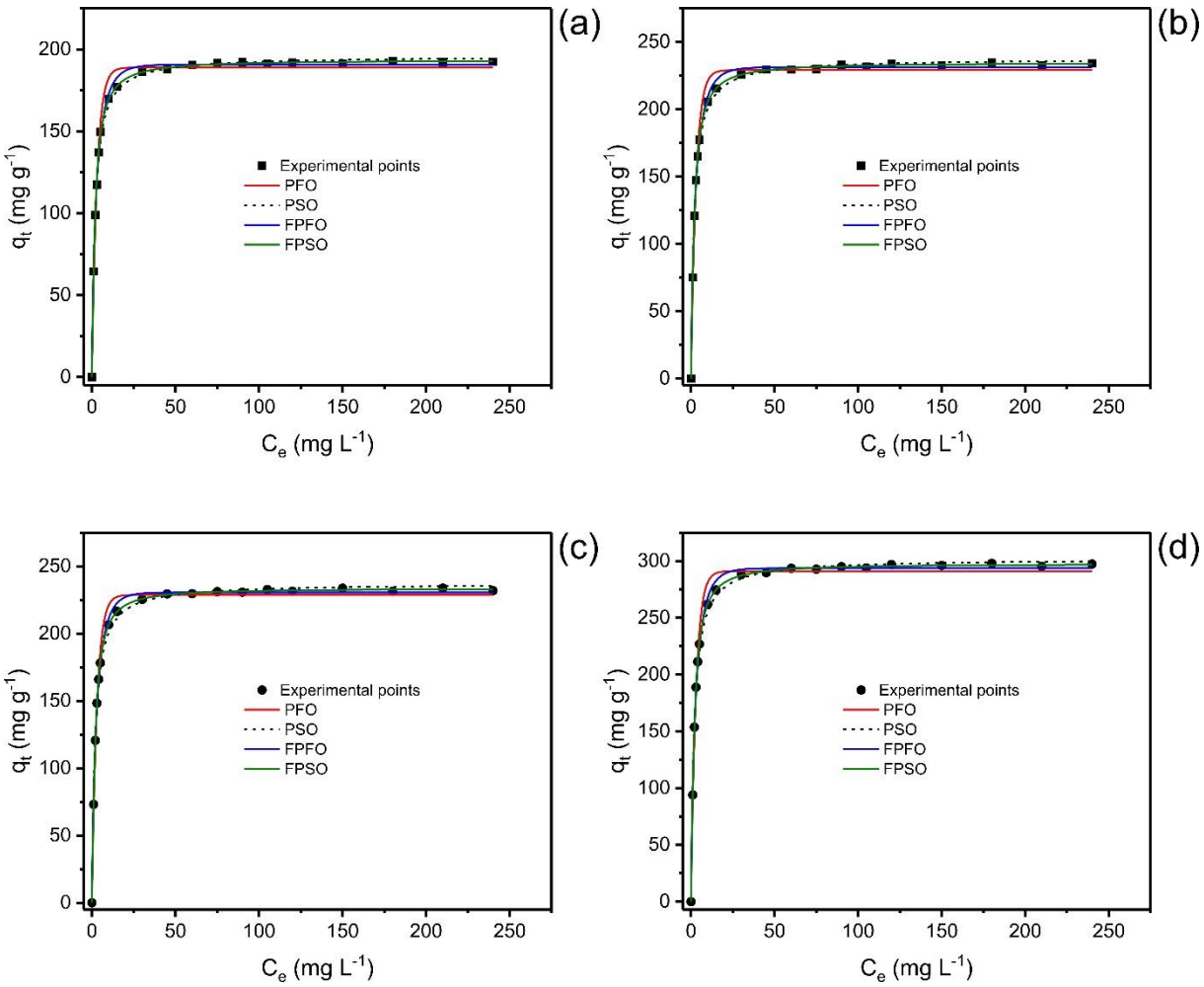

Fig 5. Kinetics of adsorption of enalapril. (a) and (c) using initial concentration of 450.0 mg L^{-1}; (b) and (d) 900.0 mg L^{-1}. (a) and (b) using BcB-1.0 and (c) and (d) using BcB-1.5 carbon material. Conditions: initial pH 7, adsorbent mass 30.0 mg, and 25°C.

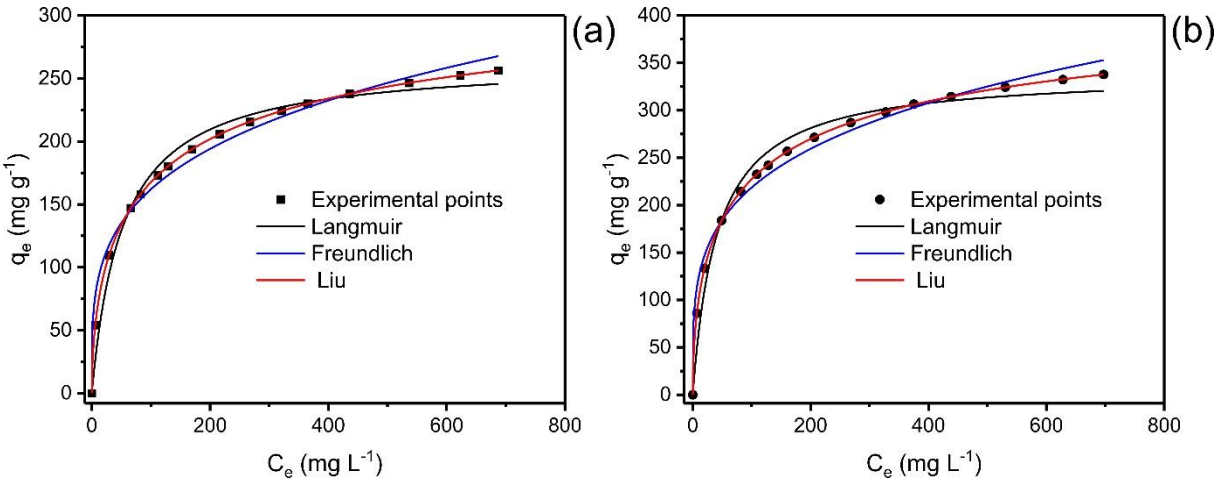

Fig 6. Enalapril adsorption isotherm. Conditions: 45°C, adsorbent mass 30.0 mg, contact time 40 min, pH 7. (a) BcB-1.0 and (b) BcB-1.5.

783

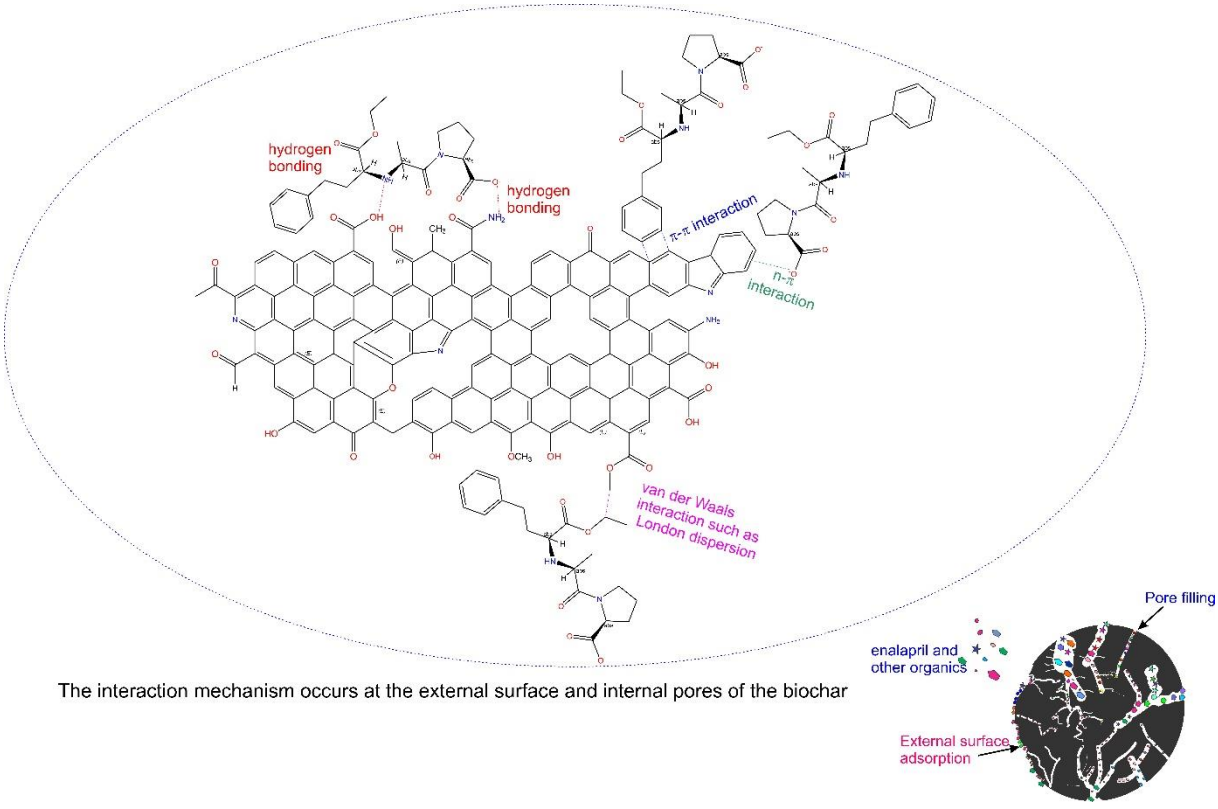

784

785 **Fig 7**. The possible interactions between enalapril and activated biochars.

786

787

788

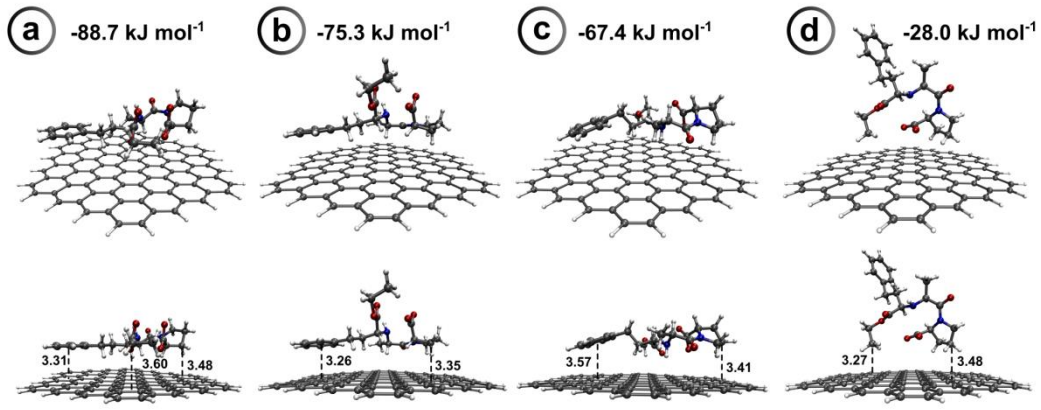

789

790 **Fig 8**. Possible adsorption configurations of enalapril on a graphitic model of biochar unraveled

791 by DFT calculations.

792

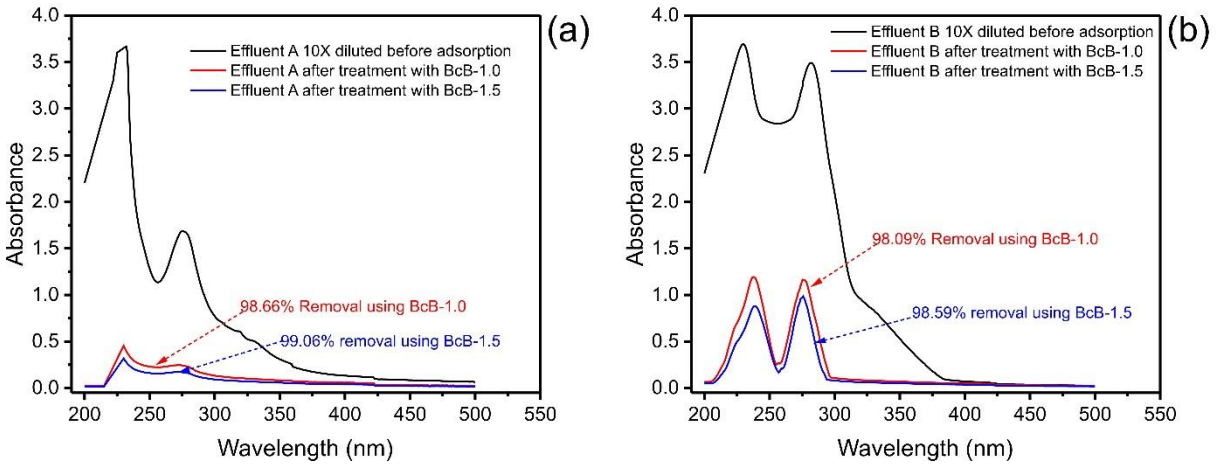

Fig 9. Synthetic pharmaceutical industry wastewaters. The absorption spectra before and after adsorption. (a) Effluent A; (b) Effluent B. Conditions: 25°C, adsorbent mass 30.0 mg, contact time 40 min.